View metadata, citation and similar papers at core.ac.uk

brought to you by CORE

provided by UNT Digital Library

LAWRENCE
LIVERMORE
NATIONAL
LABORATORY

UCRL-JRNL-212326

Model-based Processing of Microcantilever Sensor Arrays

J. W. Tringe, D. S. Clague, J. V. Candy, A. K. Sinensky, C. L. Lee, R. E. Rudd, A. K. Burnham

May 17, 2005

The Institute of Electrical and Electronics Engineers Journal of Microelectromechanical Systems

Disclaimer

This document was prepared as an account of work sponsored by an agency of the United States Government. Neither the United States Government nor the University of California nor any of their employees, makes any warranty, express or implied, or assumes any legal liability or responsibility for the accuracy, completeness, or usefulness of any information, apparatus, product, or process disclosed, or represents that its use would not infringe privately owned rights. Reference herein to any specific commercial product, process, or service by trade name, trademark, manufacturer, or otherwise, does not necessarily constitute or imply its endorsement, recommendation, or favoring by the United States Government or the University of California. The views and opinions of authors expressed herein do not necessarily state or reflect those of the United States Government or the University of California, and shall not be used for advertising or product endorsement purposes.

Model-based Processing of Microcantilever Sensor Arrays

J. W. Tringe, *Member, IEEE*, D. S. Clague, J. V. Candy, *Fellow, IEEE*,

A. K. Sinensky, C. L. Lee, R. E. Rudd, A. K. Burnham

Abstract— **We have developed a model-based processor (MBP) for a microcantilever-array sensor to detect target species in solution. We perform a proof-of-concept experiment, fit model parameters to the measured data and use them to develop a Gauss-Markov simulation. We then investigate two cases of interest, averaged deflection data and multi-channel data. For this evaluation we extract model parameters via a model-based estimation, perform a Gauss-Markov simulation, design the optimal MBP and apply it to measured experimental data. The performance of the MBP in the multi-channel case is evaluated by comparison to a "smoother" (averager) typically used for microcantilever signal analysis. It is shown that the MBP not only provides a significant gain (~ 80dB) in signal-to-noise ratio (SNR), but also consistently outperforms the smoother by 40-60 dB. Finally, we apply the processor to the smoothed experimental data and demonstrate its capability for chemical detection. The MBP performs quite well, apart from a correctable systematic bias error.**

***Index Terms*—Microcantilever, model-based processor, sensor, signal processing**

I. Introduction

MICROMACHINED cantilevers are powerful transducers for sensing inorganic, organic and biological molecules, since they readily deflect in the presence of a very small number of target molecules (nanomolar to femtomolar concentrations).[1, 2] The number of potential target chemicals is large, ranging from DNA [3, 4] to explosives [5], suggesting that cantilevers may be useful in defense, medicine, drug discovery, and environmental monitoring. Microcantilevers have already been demonstrated to be capable of recognizing antibodies [6] and nerve agent products such as hydrofluoric acid in solution [2], for example. Many other cantilever-based sensors have been developed recently [7-9]; their function and application are reviewed elsewhere.[10, 11]

A limitation on cantilever sensors in liquid, however, is that their signal-to-noise ratio (SNR) is low, often 5:1 or smaller. SNR is expected to be significantly lower in many operational environments of interest. Further, the reliability of fielded cantilever sensors ultimately depends on their being incorporated into arrays, which increase system complexity and can make response interpretation difficult. Fortunately, these difficulties are exactly the type that can be overcome with effective signal extraction techniques such as the model-based approach. Control levers and cantilevers functionalized in complementary schemes have previously been employed in arrays to improve the overall sensor sensitivity and selectivity. [1, 12, 13] Here, a model-based signal extraction system for cantilever arrays is described that takes advantage of multiple redundant signals available to the signal processing algorithm. This approach improves the SNR and helps provide a physical basis for interpreting the deflection signal.

Funding for this work came from an NA-22 Exploratory Research Program managed by David Dye. This work was performed under the auspices of the Department of Energy by the University of California/Lawrence Livermore National Laboratory under Contract W-7405-ENG-48.

All authors are with the University of California, Lawrence Livermore National Laboratory, L-234, Livermore, CA 94550, USA (phone: 925-422-7725; fax: 925-422-2041; e-mail: tringe2@llnl.gov.)

This paper discusses the development of a model-based processor (MBP) designed to extract cantilever deflection signals in low SNR environments. In Sec. II, we develop the cantilever sensor model used in the MBP along with the physical chemistry required to predict the surface concentration and stress in the subsequent section. Next, the experiment to validate the models and develop the MBP is briefly discussed in Sec. IV. The approach to model-based signal processing follows in Sec. V as well as the details of constructing the corresponding processor for this application. The MBP performance is evaluated and applied to both synthesized and experimental measurement data.

II. MICROCANTILEVER SENSORS

Micromachined cantilevers can function as detection devices when one side is fabricated to be chemically distinct from the other, as shown in Fig. 1. Functionalization can be accomplished, for example, by evaporating a thin (~10's of nm) film of metal such as Au on the top of the chip, then immersing the cantilever chip in a "probe" chemical that will bind preferentially to the Au thin film. The lever acts as a sensor when it is exposed to a second "target" chemical that reacts with the probe, since the reaction causes a free energy change that induces stress at the cantilever surface. Differential surface stress, $\Delta\sigma$ ($=\sigma^{+}-\sigma^{-}$, from Fig. 1), in turn, induces a deflection of the cantilever that can be measured optically or electronically. In this paper, we describe results of experiments with Au-coated cantilevers exposed to 2-mercaptoethanol (C_2H_6OS), a small sulfur-terminated molecule with high affinity for Au. We note that the signal-processing approach developed here should apply well to cantilevers that are functionalized to promote the binding of other chemicals or biological molecules.

The total free energy change of the cantilever surface, ΔG, can be decomposed into four contributions: ΔG_{CANT}, the mechanical energy change associated with bending the cantilever, ΔG_{POLY}, free energy change resulting from macromolecular conformational entropy and non-electrostatic interactions, ΔG_{OSM}, free energy change from osmotic pressure of counter-ions near the surface of the cantilever, and ΔG_{ELEC}, the electrostatic free energy change[3].

$$\Delta G = \Delta G_{CANT} + \Delta G_{POLY} + \Delta G_{OSM} + \Delta G_{ELEC} \tag{1}$$

The free energy change is related to $\Delta\sigma$, the surface stress difference between top and bottom side of the cantilever by:

$$\Delta\sigma(t) = \Delta G(t)\Gamma(t) / M_A \tag{2}$$

where ΔG has units of J/mole and is the change in the sum of all of the contributions to the free energy of the surface of the cantilever, $\Gamma(t)$ is the surface concentration of the species of interest (typically in molecules per cm^2) on the surface of the cantilever [14, 15]and M_A is Avogadro's number. Sulfur-terminated molecules bind preferentially to the Au-coated side of the cantilever.

The surface concentration of the interacting molecules, $\Gamma(t)$, is estimated using Langmuir kinetics. The equation describing first-order Langmuir kinetics has the following form:

$$\frac{d\left(\frac{\Gamma(t)}{\Gamma_{max}}\right)}{dt} = k_a c(t)\left(1 - \frac{\Gamma(t)}{\Gamma_{max}}\right) - k_d' \Gamma(t) \tag{3}$$

Here c(t) is the bulk concentration of the target molecule in solution in moles per liter, or [M], k_a is the adsorption rate constant in $[M]^{-1}\ s^{-1}$, k_d' ($= k_d/\Gamma_{max}$) is the desorption rate constant in $cm^2\ molecule^{-1}\ s^{-1}$. Γ_{max} is the maximum possible surface

concentration of the species of interest in molecules cm^{-2}, which is approached asymptotically at equilibrium as the solution concentration becomes very large. Finally, differential surface stress, from (2), in the cantilever induces a deflection, $\Delta z(t)$, using a variant of Stoney's equation[16]:

$$\Delta z(t) = \frac{3l^2(1-\nu)}{E\delta^2}\Delta\sigma(t), \quad (4)$$

where E is the Young's modulus, ν is the Poisson's ratio, and l and δ are the cantilever length and thickness, respectively. The terms multiplying the differential surface stress are system-specific constants and can be combined and expressed as a single coefficient,

$$\Delta z(t)=\beta\Delta\sigma(t) \quad (5)$$

$$\text{Here, } \beta=3l^2(1-\nu)/(E\delta^2). \quad (6)$$

The proportionality constant that relates cantilever deflection, $\Delta z(t)$, to induced surface stress due to surface coverage, $\Delta\sigma(t)$, can be written equivalently in terms of the spring constant of the rectangular cantilever, $k_{rect,}= E\delta^3W/(4l^3)$[17]:

$$\Delta z_i^c(t) = \frac{3(1-\nu)}{4}\frac{W\delta}{l}\frac{1}{k_{rect}}\Delta\sigma_i(t) \quad (7)$$

where W is the width of the cantilever. Correspondingly, the coefficient to the surface stress, β, given above can be re-written as,

$$\beta = \frac{3(1-\nu)W\delta}{4lk_{rect}} \quad . \quad (8)$$

The equations describing the cantilever deflection (4-8) assume that the strain is small, an assumption that is valid for all of the deflections encountered in our experiments.

III. PHYSICAL CHEMISTRY AND THERMAL EFFECTS

In this section, we describe how we predict changes in surface stress as a function of surface loading. The analysis also begins with Stoney's equation (4), which states that the deflection of the cantilever is directly proportional to the difference in surface stress on the cantilever surface. This stress differential constitutes the signal. We follow the approach as described by Lavrik et al.[15] to relate the surface stress difference to the surface coverage and the free energy of adsorption (2). What remains is to develop physical models for $\Gamma(t)$ and ΔG.

When incorporating the rate of change of the dimensionless surface concentration, $\Gamma(t)/\Gamma_{max}$, for the MBP, we employ a modified form of (3) by re-defining a rate of desorption, k_d , where $k_d = k_d^{'}\Gamma_{\max}$ and has units of s^{-1}. With this new definition (3) becomes:

$$\frac{d\left(\frac{\Gamma(t)}{\Gamma_{\max}}\right)}{dt} = k_a c(t)\left(1-\frac{\Gamma(t)}{\Gamma_{\max}}\right) - k_d\frac{\Gamma(t)}{\Gamma_{\max}} \quad (9)$$

All terms are as described above in (3) with the exception of k_d . Note that Langmuir kinetic equations have been presented in various forms in the literature. This form, (9), was chosen to enable a one-to-one comparison between rate constants predicted by the MBP presented here and those reported in the literature [18-20].

Once the input signal, a bulk concentration c_0 of target molecules, is turned off, we fit the desorption process with an nth order Langmuir desorption model:

$$\frac{d\left(\frac{\Gamma_i(t)}{\Gamma_{\max}}\right)}{dt} = -k_d\left(\frac{\Gamma_i(t)}{\Gamma_{\max}}\right)^n \tag{10}$$

The fit to the actual desorption data revealed a third-order dependence on the surface concentration, or n = 3 (see Section IV: Experimental Results). Desorption processes are typically modeled with a first or second order model to extract k_d, and the preference for a third order model is somewhat surprising. The higher order behavior could indicate a cooperative desorption process, but it is more likely due to a distribution of activation energies associated with the desorption process [21].

Also included in the model-based processor is the cantilever response to thermal effects, deflections due to differences in the coefficient of thermal expansion of Au and Si. Thermally-induced deflections are added directly to chemically-induced deflections to obtain the total cantilever deflection. From [22],

$$\Delta z^T = 3\Delta\alpha l^2 \frac{\delta_{Au} + \delta_{Si}}{\delta_{Si}^{\ 2} k_1}\Delta T \tag{11}$$

where Δz^T is the normal (z-direction) deflection of the free end of the cantilever, ΔT is the temperature difference, $\Delta\alpha$ is the difference in thermal expansion coefficients ($\alpha_{Si} - \alpha_{Au}$), l is the cantilever length, δ is the thickness of the Si or Au, and k_1 is

$$k_1 = 4 + 6\frac{\delta_{Au}}{\delta_{Si}} + 4\left(\frac{\delta_{Au}}{\delta_{Si}}\right)^2 + \frac{E_{Au}}{E_{Si}}\frac{(1-\nu_{Si})}{(1-\nu_{Au})}\left(\frac{\delta_{Au}}{\delta_{Si}}\right)^3 + \frac{E_{Si}}{E_{Au}}\frac{(1-\nu_{Au})}{(1-\nu_{Si})}\left(\frac{\delta_{Si}}{\delta_{Au}}\right) \tag{12}$$

Here E is Young's modulus for Si or Au, and ν is Poisson's ratio for Si or Au. Note the Poisson effect has been included in k_1, and that the gold layer is relatively thin so the final term dominates the expression for k_1.

The models describing the physics of the cantilever bending and the surface chemistry were built into the model-based signal processor, and a parameter estimator was developed to fit these coupled equations predicting the optimal values for k_a, k_d and $\Gamma_{max.}$ With these parameters specified, we calculate the free energy for adsorption, $\Delta G_{ads} = -RT\ln\left(\frac{k_a}{k_d}\right)$ [18, 20]. For any target species, we can then fit to find the appropriate adsorption parameters.

IV. Experimental Results

A prototype cantilever detection system from Veeco Instruments, Inc., was used for these experiments. In this system, a single Si chip (fabricated by IBM) with eight identical cantilevers is loaded into a 50 microliter flow cell, and cantilever deflections are measured optically using a focused light beam from a super-luminescent diode reflected into a position-sensitive detector by

each cantilever. Levers are interrogated in series, with an overall measurement frequency of ~2 Hz for all eight levers. Each Si cantilever is 500 microns long, 100 microns wide and 1 micron thick; levers are parallel to one another on the chip, spaced by 100 microns. The top side of the levers (as depicted in Fig. 1) was coated with 20 nm of evaporated Au on a 2.5 nm Ti adhesion layer, and the whole chip was cleaned with piranha (3:1 H_2SO_4:30% H_2O_2) immediately before being loaded into a water-filled 50 microliter flow cell.

During the experiment, levers were exposed to a thermal pulse, then a chemical stimulus in the form of a $c_0 = 0.014$ M concentration of 2-mercaptoethanol in pure water, and finally a second heat pulse. Except for brief pauses to exchange syringes in the syringe pump, the entire experiment was performed at a constant flow rate of 20 microliter/min. Results of this experiment are shown in Fig. 2: the average deflection of 6 of 8 cantilevers (2 others were damaged), and simultaneous temperature measurements from a thermocouple placed in the flow of fluid exiting the cell. Similar experiments were repeated several times, and the data shown are typical of the magnitude and time evolution of the deflection and temperature signals.

V. MODEL-BASED SIGNAL PROCESSING

A. Design for cantilever arrays

In this section we develop the model-based approach, first for the generic model sets and then for the specific embellishment discussed previously. We start the section with the development of an approximate Gauss-Markov model, which can be used to capture the general cantilever signal enhancement problem. We then apply it to our specific microcantilever array sensor system.

If nonlinear dynamics (differential equations) describe the system under investigation, then an approximate representation of the deterministic process and associated measurement is easily captured in state-space form. State-space is simply converting an n^{th}-order set of coupled differential equations into an equivalent set of n first-order differential equations. With this accomplished, we obtain the general nonlinear vector functional relations defined by the *process and measurement models*,

$$\begin{aligned} \dot{x}(t) &= a[x,u;\theta] && \text{[process (state)]} \\ y(t) &= c[x,u;\theta] && \text{[measurement]} \end{aligned} \tag{13}$$

where x is the N_x-dimensional state vector; y is the N_y-dimensional measurement. u is a known input, and θ is a generic model parameter. If these processes are contaminated by additive zero-mean, Gaussian noise, then the approximate Gauss-Markov model evolves as

$$\begin{aligned} \dot{x}(t) &= a[x,u;\theta]+\mathrm{w(t)} && \text{[process (state)]} \\ y(t) &= c[x,u;\theta]+\mathrm{v(t)} && \text{[measurement]} \end{aligned} \tag{14}$$

Here $a[\cdot]$, $c[\cdot]$ are the N_x-dimensional vector process function and N_y-dimensional measurement functions, respectively, for the process noise given by $w \sim N(0, R_{ww})$ and the corresponding measurement noise, $v \sim N(0, R_{vv})$. $N(\cdot,\cdot)$ is the Gaussian distribution specified by mean and covariance. With this representation in mind, we can now define the generic *cantilever signal enhancement* problem as:

GIVEN a set of noisy displacement measurements, $\{y(t)\}$ with known inputs, $\{u(t)\}$,and parameters, $\{\theta\}$, specified by the approximate Gauss-Markov model of (14), FIND the best (minimum error variance) estimate of the displacement and surface concentrations, $\hat{y}(t)$, $\hat{x}(t)$, respectively.

The solution to this problem can be derived in a wide variety of approaches. Here, we will use the common Bayesian approach [23]. We summarize the algorithm as:

MODEL-BASED PROCESSOR ALGORITHM

$$\dot{\hat{x}}(t\,|\,t-1) = a\left[\hat{x}, u; \theta\right] \quad \text{[State Prediction]}$$

$$\hat{y}(t\,|\,t-1) = c\left[\hat{x}, u; \theta\right] \quad \text{[Measurement Prediction]} \qquad (15)$$

$$\varepsilon(t) = y(t) - \hat{y}(t\,|\,t-1) \quad \text{[Innovation or Residual]}$$

$$\hat{x}(t\,|\,t) = \hat{x}(t\,|\,t-1) + K(t)\varepsilon(t) \quad \text{[Correction]}$$

where $K(t)$ is the gain of the processor, which must be calculated from the underlying process statistics (see [23] for details). Here we have discretized time and measured it in units of the time step, so the time at the step before *t* is *t*-1.

For the cantilever array problem, we must convert the physical relations, (2-12), into the state-space form above. We chose to solve the differential equation and incorporate the resulting relations into the measurement (cantilever sensor) model. For the state, we modeled the free energy as a piecewise constant function, converted it to discrete-time using the first difference approximation and excited it with zero-mean, white Gaussian (process) noise creating a random walk model for this parameter. Therefore, we start with defining the state vector as $x := \Delta G$ and the deflection measurement y := Δz; then we obtain the following relations. From (14), the surface concentration relation becomes simply

$$x(t) = x(t-1) \quad \text{[Process Model]} \qquad (16)$$

The measurement model is more complicated. We must first solve for the physical variables to obtain the generic form of (11); therefore, we have from (2-12) that

$$y_i(t) = \Delta z_i^c(t) + \Delta z^T(t) \quad \text{[Measurement Model]} \qquad (17)$$

where $\Delta z_i^c(t)$ is the chemically-induced deflection, different for different cantilevers. $\Delta z^T(t)$ thermal deflection, assumed to be the same for all cantilevers. In addition to accounting for the adsorption-desorption kinetics, we also developed an approximation, based on the stirred tank reactor, to estimate the target concentration as a function of time under continuous flow conditions. In the experiments presented in this communication the applied chemical signal was a step function, i.e., a constant concentration at was turned on at time, t_{ON}, and off at time t_{OFF}.[24] The dynamic surface concentration, Γ(t), has the following form:

$$\begin{aligned}
\Gamma(t)/\Gamma_{\max} &= 0, && t < t_{ON} \\
\Gamma(t)/\Gamma_{\max} &= \left(\frac{c(t)}{c(t)+k_a/k_d}\right)\{1-\exp[-(k_a c(t)+k_d)(t-t_{ON})]\}, && t_{ON} \le t \le t_{OFF} \\
\Gamma(t)/\Gamma_{\max} &= \sqrt{\frac{1}{2k_d(t-t_{OFF})}}, && t > t_{OFF}
\end{aligned} \tag{18}$$

As described above, the differential surface stress on the cantilever is a function of the surface concentration and free energy

$$\Delta\sigma(t) = \Gamma(t)\Delta G(t) = \Gamma(t)x(t) \tag{19}$$

The deflection of the i^{th} -lever is weighted by the Stoney equation with a specific value of β, from (5):

$$\Delta z_i^c(t) = \beta_i \Delta\sigma(t), \text{ for } \beta_i := 3l^2(1-\nu)/(E_i\delta_i^2) \tag{20}$$

where β_i is the i^{th} -Stoney coefficient with cantilever modulus, E_i , with lever length and thickness, l and δ_i, respectively, and ν is Poisson's ratio for silicon. Here we allow different values of β for the different cantilevers to account for the well-known variations in cantilever properties, something that has been investigated extensively in the context of AFM cantilever spring constants. In principle, variations in either E [25]or δ [26] could cause appreciable variations in β; in practice, the variation of the Young's modulus of silicon is much less than the variation of δ^2. Fortunately, it is the same combination ($E\,\delta^2$) that enters both β and the leading term of k_1, so a single fitting parameter suffices to account for variations in both. In practice we have taken this parameter to be E_i. Thus, we obtain the measurement equation at the i^{th} -cantilever as

$$y_i(t) = \beta_i\Gamma(t)x(t) + \Delta z^T(t) \tag{21}$$

Finally, assuming that both noise sources are Gaussian random processes (as before), then the result is a time-varying Gauss-Markov (not approximate due to linearity) multi-channel cantilever model defined by

$$\begin{aligned}
x(t) &= x(t-1) + w(t-1) \\
yi(t) &= \beta_i\Gamma(t)x(t) + \Delta z^T(t) + \nu_i(t)
\end{aligned} \tag{22}$$

for $w \sim N(0, R_{ww})$; $v \sim N(0, R_{vv})$. As before, we can develop the model-based processor based on this Gauss-Markov model. First, we define the signal enhancement problem in terms of the cantilever models as:

> GIVEN a set of noisy N_y -vector displacement measurements, $\{\mathbf{y}(t)\}$ with known N_u -vector inputs, $\{\mathbf{u}(t)\}$ and parameters, $\{\theta_k\}$ specified by the Gauss-Markov model of (14), FIND the best (minimum error variance) estimate of the displacement and N_x -vector surface concentrations, $\hat{\mathbf{y}}(t\,|\,t-1)$, $\hat{\mathbf{x}}(t\,|\,t)$, respectively.

The model-based algorithm to solve this problem using the specified models is:

CANTILEVER ARRAY MODEL-BASED PROCESSOR ALGORITHM

$$\begin{aligned}
\hat{x}(t|t-1) &= \hat{x}(t-1|t-1) && \text{[Surface Concentration Prediction]} \\
\hat{y}_i(t|t-1) &= \beta_i\Gamma(t)\hat{x}(t|t-1) + \hat{\tau}(t) && \text{[Displacement Prediction]} \\
\varepsilon_i(t) &= y_i(t) - \hat{y}_i(t|t-1) && \text{[Innovation or Residual]}
\end{aligned} \tag{23}$$

$$\hat{x}(t|t-1) = \hat{x}(t-1|t-1) + k(t)\varepsilon(t) \qquad \text{[Surface Concentration Correction]}$$

This completes the development of the MBP algorithm for cantilever sensor arrays. Note that once this framework is developed, it is straightforward to define other problems of high interest (e.g. detection problems[27]).

B. Model-based processor performance evaluation

In this section we discuss the performance of the model-based processor (MBP) for signal enhancement of an *L*-element cantilever sensor array. The basic approach we take for MBP performance evaluation is illustrated in Fig. 3. After obtaining the average parameters by performing the parameter estimation, a Gauss-Markov simulation was designed to generate synthesized cantilever deflection measurements using the model discussed in the previous section. Once synthesized at a particular signal-to-noise ratio (SNR), the processors were applied to the data and their performance analyzed based on the "truth" deflections generated by a noise-free simulation. Metrics are applied to evaluate and compare performance. We discuss the various steps in this procedure.

1) Parameter Estimation. The basic approach we use is to first "parameterize" the cantilever array model by performing parameter estimation (nonlinear least squares method) on the raw deflection measurements to extract the critical absorption, desorption and maximum concentration, that is, $\theta_i = \{k_a(i), k_d(i), \Gamma_{\max}(i)\}; \quad i = 1, \cdots, L$. The parameter estimator we employed was a nonlinear least-squares criterion using the Nelder-Meade polytope search algorithm[28]. This algorithm is based on minimizing

$$\min_{\theta_i} J(\theta) = \sum_{t=1}^{N_t} \varepsilon_i^2(t;\theta) \quad \text{for} \quad \varepsilon(t;\theta) \coloneqq y_i(t) - \hat{y}_i(t;\theta), \tag{24}$$

where the estimated or filtered cantilever measurement at the i^{th} -lever is given by

$$\hat{y}_i(t;\theta) = \Delta z_i^c(t;\theta) + \Delta z^T(t) \tag{25}$$

Once these parameters are extracted from the data, they are averaged to give $\bar{\boldsymbol{\theta}} = \{\overline{k_a}, \overline{k_d}, \overline{\Gamma_{max}}\}$. These are the parameters that are used in the Gauss-Markov simulation model.

We tested the parameter estimator with raw experimental deflection data (Fig. 2) to determine the appropriate physical parameters for each lever on a single chip. Modeling results are shown in Fig. 4 where we see the "fitted" deflection responses compared to the measured. It is clear that the extracted parameters reasonably predict the filtered cantilever response of (25). Next we investigate the development of the simulator.

2) Gauss-Markov Model Simulation. For our problem we chose to use $\Delta G(t)$ as an unknown but constant parameter ($\frac{d\Delta G(t)}{dt} = 0$) and the nonlinear deflection and known temperature measurement; that is, defining

$$\Delta G(t) = \Delta G(t-1) + w(t-1) \tag{26}$$

with cantilever array measurement

$$y_i(t) = \beta_i \Gamma(t) \Delta G(t) + \Delta z^T(t) + \nu_i(t) \tag{27}$$

where $\Delta G(t)$ is the free energy at the surface, and w, v_i are the additive, zero-mean, Gaussian noise processes with covariances, R_{ww} and $R_{vv} \in \mathbf{R}^{L\times L}$ with diagonals, $\sigma_v^2(i);\ \ i=1,\cdots,L$. We assume that the measurement uncertainty is uncorrelated producing the diagonal matrix. Each of the cantilevers has a different value of β creating a set of Stoney coefficients, $\beta \rightarrow \beta_i$, one representing each of the individual lever properties. A typical set of cantilever simulation data is shown in Fig. 5 where we used a *–20 dB* SNR defined by:

$$SNR_i = \frac{\sigma^2_{\Delta z,true}(i)}{\sigma_v^2(i)};\ \ i=1,\cdots,L \tag{28}$$

where Δz_{true} is the "true" deflection available from the Gauss-Markov simulation and $\sigma^2_{\Delta z,true}$ is its variance. Once the noisy deflection measurements are synthesized, then the processors are applied to extract the "true" deflections. We chose to evaluate two methods: smoothing processor and model-based processor. The smoothing processor is simply a running window average that is equivalent to a low-pass filtering operation. This smoothing is an example of a typical approach taken by scientists in this field. The MBP is the "optimal" (approximately) solution to this problem. We used *SSPACK_PC,* a commercial model-based signal processing package[29] in MATLAB[30], to perform these calculations. Table 1 gives values parameters for the cantilever used in the calculations.

C. MBP application to single channel cantilever data

The MBP was developed using the cantilever measurement model of (29) with the average parameter estimates of Table II. Concerning the values given in Table II, it is helpful to review results obtained in related chemical systems. For example, k_a is 1.3×10^{-2} s^{-1} for CH_3 $(CH_2)_{15}$ S/Au (10^{-3} M) in ethanol, relatively constant between concentrations of 10^{-3} and 10^{-5} M [31]; our average value of 4.6×10^{-3} s^{-1} for k_a for 2-mercaptoethanol, C_2H_6OS, (1.4×10^{-2} M) in water is smaller, possibly because of different kinetic mechanisms that are active for this smaller molecule at higher concentrations, or because of solvent differences. Unlike the longer CH_3 $(CH_2)_{15}$ S, for example, 2-mercaptoethanol does not form well-ordered monolayers on Au. For 20-base pair thiolated DNA on Au in buffer, k_d is 4.7×10^{-3} s^{-1}, and $\Gamma_{max} = 1.3\times10^{13}$ molecule/cm^2 [1]. Our value of 4.8×10^{-4} s^{-1} for k_d is smaller, again possibly because of molecular size or solvent differences. Γ_{max} for C_2H_6OS is larger (1.3×10^{15} molecule/cm^2), likely because the much smaller C_2H_6OS is better able to concentrate on the Au surface.

In this section we discuss the application of the MBP to simulated cantilever array measurement data at a variety of signal-to-noise ratios. We first show the results of the MBP design for the *–20 dB* SNR case, then summarize the results at a variety of signal-to-noise ratios to evaluate its overall performance. The MBP design is based not only on the average parameter estimates (see Table II), but also using a smoothed temperature data estimate, $\Delta\hat{z}^T(t)$, to be more realistic in performance evaluation. We expect this processor to provide an outstanding performance, once tuned[23]. In fact, the results of applying it to the *–20 dB* data indicate an approximate optimal performance, since the underlying prediction errors or innovations associated with each lever are statistically zero-mean (mean less than bound) and white (less than 5% of the points outside the bound) as shown in Fig. 6 and Table III. To pass in Table III, simulated data must be zero-mean and white. Table III also shows the aggregated weighted-sum squared residual (WSSR) statistic indicating optimal performance. The results of processing the *–20 dB* SNR deflection data are shown in Fig. 7 for each lever. The results are shown by comparing the "true" (synthesized) deflection compared to the smoothed and MBP estimates. It is clear from the figure that the MBP performs extremely well.

Next we investigate the overall performance of both the standard smoother/averager and the MBP on synthesized data sets. In order to quantitatively evaluate the performance of the processors individually, we calculate the residual deflection errors defined by

$$\Delta\tilde{z}_i^c(t) := \Delta z_{true,i}^c(t) - \Delta\hat{z}_i^c(t) \tag{29}$$

where $\Delta z_{true,i}^c(t)$ is the true (noise free) deflection at the i^{th} -lever and $\Delta\hat{z}_i^c(t)$ is the filtered or estimated deflections as shown for the *–20 dB* case in Fig. 7. Once the error is estimated at each lever, its associated mean and variance can be calculated and used for further analysis. We define the *processor output gain* as the final metric given by:

$$SNR_{out}(i) := \frac{\sigma^2_{\Delta z,true}(i)}{\sigma^2_{\Delta\tilde{z},true}(i)};\quad \mathrm{i}=1,\cdots,\mathrm{L}\,. \tag{30}$$

This ratio represents the enhancement provided by each processor. The smaller the residual error variance ($\sigma^2_{\Delta\tilde{z}}$), the higher the SNR_{out} , providing a reasonable metric. Averaging these statistics over the cantilever array gives a measure of overall processing gain.

We performed a set of simulations at *0, -20, -40 dB* SNR_{in} with the typical run outputs shown in the previous figures for the *–20 dB* case. The results for each run are summarized in Table IV. Here we see that output SNR produced by both processors are respectable with a significant gain in enhancement; however, it is clear that the MBP consistently demonstrates superior performance with an overall average enhancement of *80 dB* and enhancement gain over the Smoother of *38*, *43* and *60 dB*, respectively. The MBP is *insensitive* at these SNRs to the measurement noise variance changes yielding identical performance at each level. By contrast, the Smoother performance clearly deteriorates as the input SNR decreases. The MBP performance will also deteriorate with decreases in input SNR, but not at realistic experimental levels. This demonstrates outstanding performance for multi-channel cantilever arrays on these simulated data sets. Next we apply the process to the measured array data.

D. Model-based processor application to multichannel cantilever data

In this section we developed MBP for two cases: (1) average deflection data and an averaged cantilever model; and (2) multi-channel deflection data. First we averaged the six cantilever deflection data to obtain the complete deflection response over the entire array. We next designed the MBP: we first obtained the parameter estimates, then applied those parameters to the processor. Finally, we developed the multi-channel processor using the same approach: estimating the individual cantilever parameters, taking their average and calculating the appropriate parameters for the multi-channel model. In both cases we performed simulations first to develop the optimal MBP.

The average cantilever model was developed by performing the model-based parameter estimation obtaining the adsorption, desorption and free energy, then developing the corresponding Gauss-Markov simulation model and corresponding MBP. The raw and simulated data (*0 dB*) are shown in Fig. 8a and 8b. It is clear that the measurement noise severely distorts the desired deflection signal. The enhanced MBP output (deflection) enhancement is shown in Fig. 8c along with the corresponding optimality tests in 8d, where it is apparent that the performance of the processor is indeed optimal: the corresponding innovations are zero-mean and white.

Next we applied the MBP to the actual deflection and temperature profile data shown in Fig. 9a and 9b after "tuning" the noise covariance parameters (R_{vv}) with the results shown in Fig. 9d. Here we see that the MBP is capable of tracking the

averaged cantilever deflection data quite well; however, the performance is suboptimal, since the innovation, although small, is not white. Generally, the MBP performance for this data is quite good.

Next we developed the MBP for the *multi-channel case* using the same model-based approach: simulation and application. We used the average model parameters developed over the entire cantilever array data set with the nonlinear least-squares model-based parameter estimator, then applied it to the raw cantilever data to investigate its performance. We again used the MBP with the free energy as our piecewise constant parameter (state) and the nonlinear cantilever array model with six elements. We used the smoothed estimate of the temperature profile in our estimator as in the synthesized data case. We also used the estimated the Stoney coefficients and the average parameter estimates as before.

The measured cantilever data, MBP estimates and the corresponding errors or innovations are shown in Fig. 10. Since the innovations are not zero-mean and white, the processor is not optimal; however, the results are quite reasonable except for the systematic bias error (constant) in the estimate. The dynamics appear to be captured by the model especially well in cantilever five. The offset can be adjusted by selecting various combinations of elements in the R_{vv} measurement noise covariance matrix, but this may be better suited to an adaptive implementation of the processor that will be pursued in future work. From the figure we note that the dynamics of the individual levers (on-set and off-sets) are close to the expected dynamics.

VI. CONCLUSION

We have developed a successful model-based approach to the microcantilever array signal enhancement problem. Experimental data were obtained from a multi-cantilever detection system and quantitatively analyzed with mathematical tools from physical chemistry and solid state physics. We incorporated the results of this analysis directly into the generic signal processing approach. A proof-of-concept solution was created to parameterize our theoretical model, enabling us to test an average model. This model was then used to develop the MBP for enhancing noisy cantilever measurements. We investigated data averaged over the array and the multi-channel cases.

Through simulations with additive Gaussian noise at SNR of 0, -20, and –40 dB, we demonstrated the ability of the processor to extract the cantilever deflection response with a large improvement in signal gain (~ 80 dB). We compared the performance of the processor to that of a “smoother” (averager) at several differnent signal-to-noise ratios, and the MBP demonstrated superior performance with an overall average processing gain of ~ 40-60 dB over the averager. Finally, we applied the MBP to noisy, smoothed (averaged) cantilever data and demonstrated that the processor could perform quite well except for a bias error, which is easily corrected.

To demonstrate the full utility of the MBP for chemical sensing of low levels of signature chemicals, necessary next steps are (1) verify the physical models used in this study for a variety of solvents and target molecules (2) make use of control levers, and (3) extend the experimental library to include low concentrations of chemical targets of practical interest.

ACKNOWLEDGMENT

The authors gratefully acknowledge the contributions of LLNL scientists Drs. Brad Hart, Brandon Weeks, Tim Ratto and Steve Velsko, who provided guidance on chemical sensing and cantilever experimental protocols.

References

[1] R. McKendry, J. Y. Zhang, Y. Arntz, T. Strunz, M. Hegner, H. P. Lang, M. K. Baller, U. Certa, E. Meyer, H. J. Guntherodt, and C. Gerber, "Multiple label-free biodetection and quantitative DNA-binding assays on a nanomechanical cantilever array," *Proceedings of the National Academy of Sciences of the United States of America*, vol. 99, pp. 9783-9788, 2002.

[2] Y. J. Tang, J. Fang, X. H. Xu, H. F. Ji, G. M. Brown, and T. Thundat, "Detection of femtomolar concentrations of HF using an SiO2 microcantilever," *Analytical Chemistry*, vol. 76, pp. 2478-2481, 2004.

[3] M. F. Hagan, A. Majumdar, and A. K. Chakraborty, "Nanomechanical forces generated by surface grafted DNA," *Journal of Physical Chemistry B*, vol. 106, pp. 10163-10173, 2002.

[4] M. Su, S. U. Li, and V. P. Dravid, "Microcantilever resonance-based DNA detection with nanoparticle probes," *Applied Physics Letters*, vol. 82, pp. 3562-3564, 2003.

[5] G. Muralidharan, A. Wig, L. A. Pinnaduwage, D. Hedden, T. Thundat, and R. T. Lareau, "Absorption-desorption characteristics of explosive vapors investigated with microcantilevers," *Ultramicroscopy*, vol. 97, pp. 433-439, 2003.

[6] R. Wu, K. M. Datar, T. Hansen, R. Thundat, J. Cote, and A. Majumdar, "Bioassay of prostate-specific antigen (PSA) using microcantilevers," *Nature Biotechnology*, vol. 19, pp. 856-860, 2001.

[7] Y. Min, H. Lin, D. E. Dedrick, S. Satyanarayana, A. Majumdar, A. S. Bedekar, J. W. Jenkins, and S. Sundaram, "A 2-D microcantilever array for multiplexed biomolecular analysis," *IEEE Journal of Microelectromechanical Systems*, vol. 13, pp. 290 - 299, 2004.

[8] C. A. Savran, A. W. Sparks, J. Sihler, L. Jian, W. Wan-Chen, D. E. Berlin, T. P. Burg, J. Fritz, M. A. Schmidt, and S. R. Manalis, "Fabrication and characterization of a micromechanical sensor for differential detection of nanoscale motions," *Journal of Microelectromechanical Systems*, vol. 11, pp. 703-708, 2002.

[9] P. G. Datskos and I. Sauers, "Detection of 2-mercaptoethanol using gold-coated micromachined cantilevers," *Sensors and Actuators B-Chemical*, vol. B61, pp. 75-82, 1999.

[10] R. Raiteri, M. Grattarola, H. J. Butt, and P. Skladal, "Micromechanical cantilever-based biosensors," *Sensors and Actuators B-Chemical*, vol. 79, pp. 115-126, 2001.

[11] B. M. Paddle, "Biosensors for chemical and biological agents of defence interest," *Biosensors & Bioelectronics*, vol. 11, pp. 1079-1113, 1996.

[12] M. K. Baller, H. P. Lang, J. Fritz, C. Gerber, J. K. Gimzewski, U. Drechsler, H. Rothuizen, M. Despont, P. Vettiger, F. M. Battiston, J. P. Ramseyer, P. Fornaro, E. Meyer, and H. J. Guntherodt, "A cantilever array-based artificial nose," *Ultramicroscopy*, vol. 82, pp. 1-9, 2000.

[13] F. M. Battiston, J. P. Ramseyer, H. P. Lang, M. K. Baller, C. Gerber, J. K. Gimzewski, E. Meyer, and H. J. Guntherodt, "A chemical sensor based on a microfabricated cantilever array with simultaneous resonance-frequency and bending readout," *Sensors and Actuators B-Chemical*, vol. 77, pp. 122-131, 2001.

[14] A. Halperin, A. Buhot, and E. B. Zhulina, "Sensitivity, specificity, and the hybridization isotherms of DNA chips," *Biophysical Journal*, vol. 86, pp. 718-730, 2004.

[15] N. V. Lavrik, C. A. Tipple, M. J. Sepaniak, and P. G. Datskos, "Gold nano-structures for transduction of biomolecular interactions into micometer scale movements," *Biomedical Microdevices*, vol. 3, pp. 35-44, 2001.

[16] G. G. Stoney, *Proceedings of the Royal Society of London*, vol. Series A, 1909.

[17] M. Godin, V. Tabard-Cossa, P. Grütter, and P. Williams, "Quantitative Stress Measurement using a Microcantilever," *Applied Physics Letters*, vol. 79, pp. 551-553, 2001.

[18] R. Marie, H. Jensenius, J. Thaysen, C. B. Christensen, and A. Boisen, "Adsorption kinetics and mechanical properties of thiol-modified DNA-oligos on gold investigated by microcantilever sensors," *Ultramicroscopy*, vol. 91, pp. 29-36, 2002.

[19] R. Georgiadis, K. P. Peterlinz, and A. W. Peterson, "Quantitative measurements and modeling of kinetics in nucleic acid monolayer films using SPR spectroscopy," *Journal of the American Chemical Society*, vol. 122, pp. 3166-3173, 2000.

[20] D. S. Karpovich and G. J. Blanchard, "Direct Measurement of the Adsorption-Kinetics of Alkanethiolate Self-Assembled Monolayers on a Microcrystalline Gold Surface," *Langmuir*, vol. 10, pp. 3315-3322, 1994.

[21] A. K. Burnham and R. L. Braun, "Global kinetic analysis of complex materials," *Energy and Fuels*, vol. 13, pp. 1-22, 1999.

[22] Roark and Young, "Formulas for Stress and Strain," pp. Sect. 7.2.

[23] J. V. Candy, *Model-Based Signal Processing*. New York: John Wiley, 2005.

[24] D. E. Seborg, T. F. Edgar, and D. A. Mellichamp, *Process Dynamics and Control*, vol. 2nd Edition: Wiley & Sons, 1989.

[25] A. L. Weisenhorn, P. Maivald, H. J. Butt, and P. K. Hansma, "Measuring adhesion, attraction and repulsion between surfaces in liquids with an atomic force microscope," *Physical Review B*, vol. 45, pp. 11226-32, 1992.

[26] J. P. Cleveland, S. Manne, D. Bocek, and P. K. Hansma, "A nondestructive method for determining the spring constant of cantilevers for scanning force microscopy," *Review of Scientific Instruments*, vol. 64, pp. 403-405, 1993.

[27] H. V. Trees, *Detection, Estimation and Modulation Theory*, vol. 1. New York: Wiley.

[28] P. Gill, W. Murray, and M. Wright, *Practical Optimization*. New York: Academic Press, 1981.

[29] J. Candy and P. Candy, "SSPACK_PC, a model-based signal processing package on personal computers," vol. 2, no. 3 ed: DSP Applications, 1993.

[30] MathWorks, "MATLAB Reference Guide." Boston, MA: MathWorks, Inc., 1992.

[31] K. A. Peterlinz and R. Georgiadis, "In situ kinetics of self assembly by surface plasmon resonance spectroscopy," *Langmuir*, vol. 12, pp. 4731-4740, 1996.

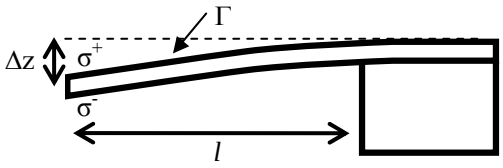

Fig. 1. Schematic side view of a micro-machined cantilever showing cantilever length, *l*, deflection, Δz, surface stress, σ^+ and σ^-, and surface concentration of target species, Γ. Adsorption of the target species on the top cantilever surface induces a measurable deflection of the cantilever.

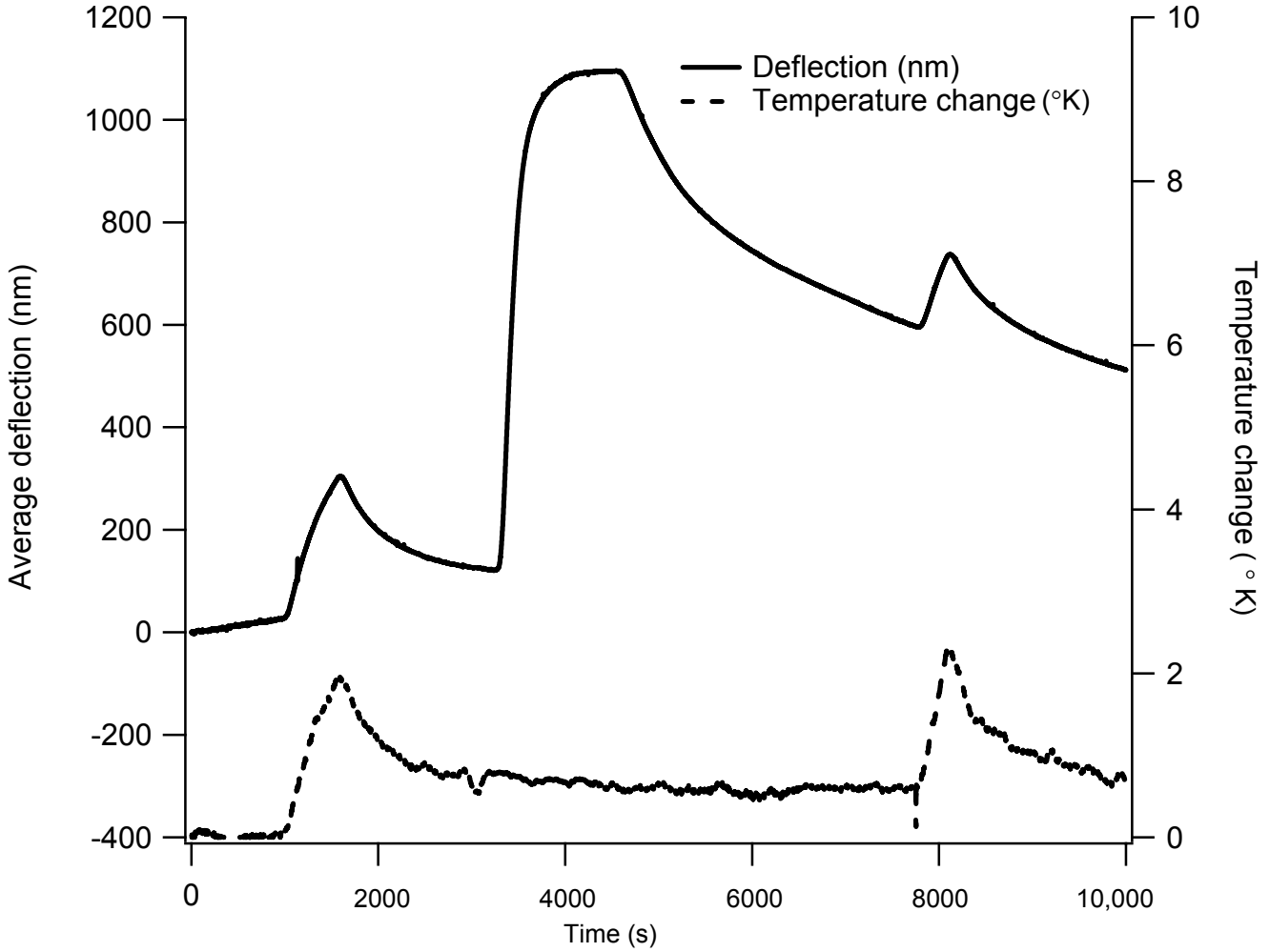

Fig. 2. Mean deflection of the cantilevers due to temperature and chemical stimuli; deflection signal is averaged over six cantilevers. The temperature change was measured in the fluid exiting the cell.

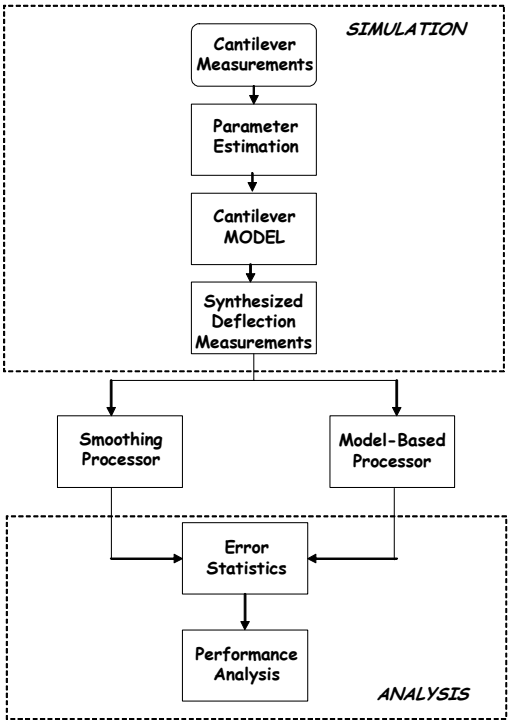

Fig. 3. Model-Based Processor Performance Evaluation: Simulation, Processing and Analysis. This approach allows direct comparison of the results of the smoothing processor and the MBP.

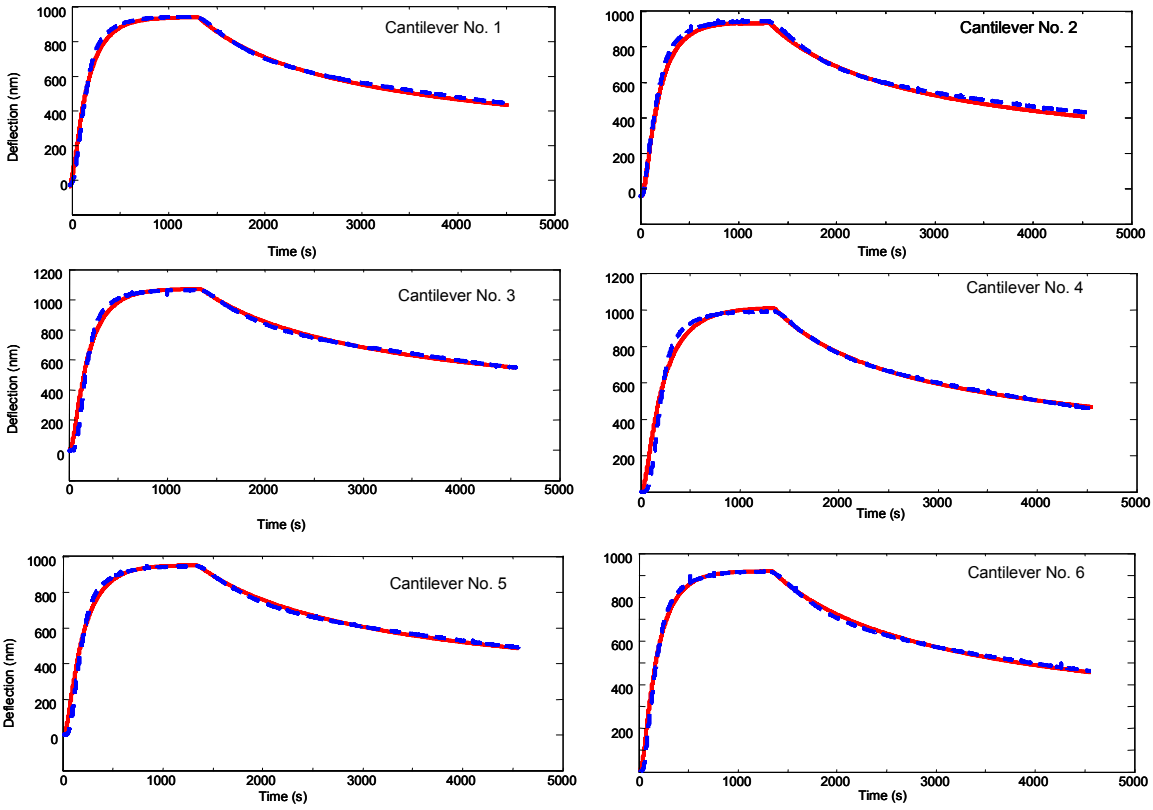

Fig. 4. Parameter Estimator Results: Predicted response (solid line) compared to raw deflection measurements (dotted line). The concentration, c_0, is 0.014 M, 2-mercaptoethanol in water.

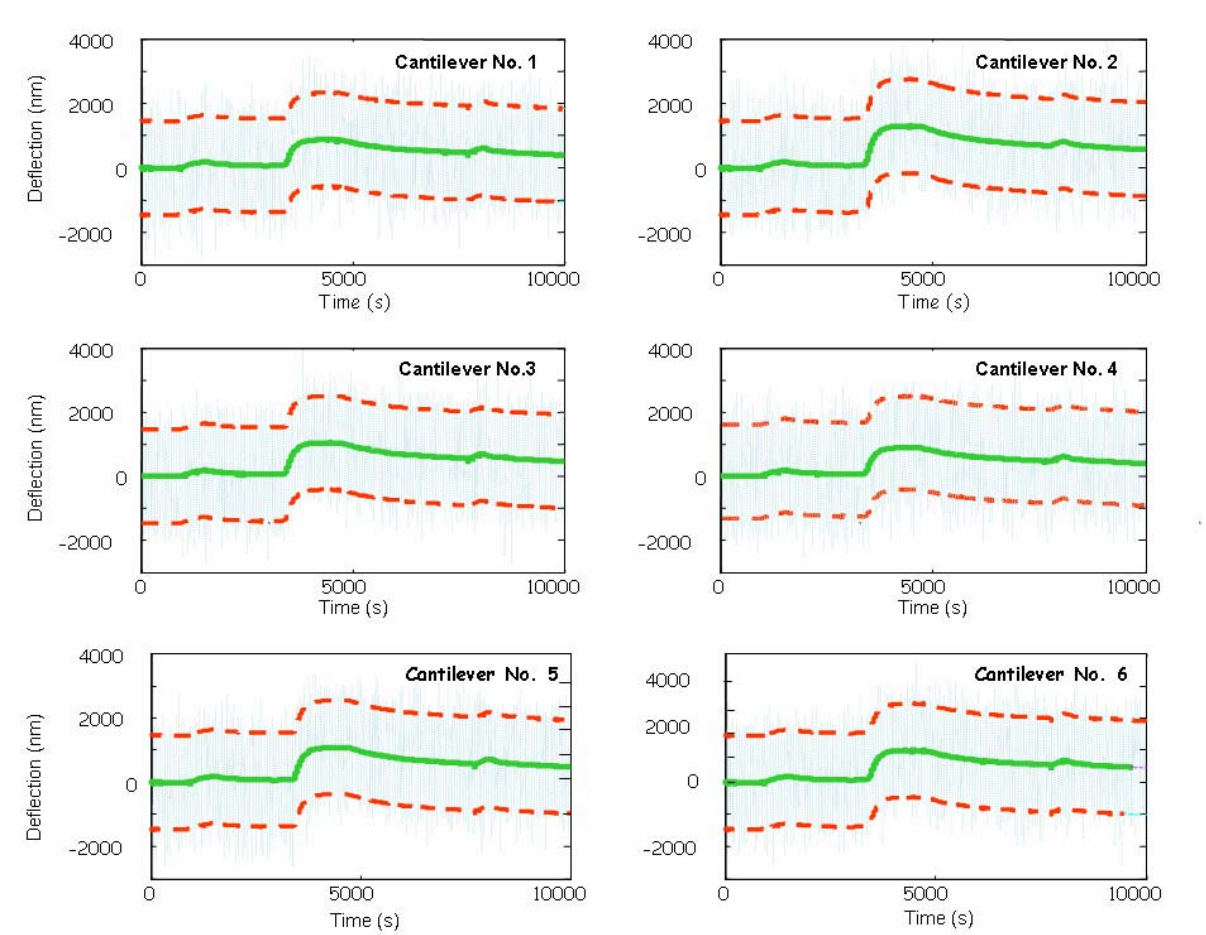

Fig. 5: Noisy Cantilever Deflection Measurement Gauss Markov Simulation (-20 dB SNR). In each chart, the solid green center line is the mean deflection, while the red dashed lines are the twice the standard deviation from the mean.

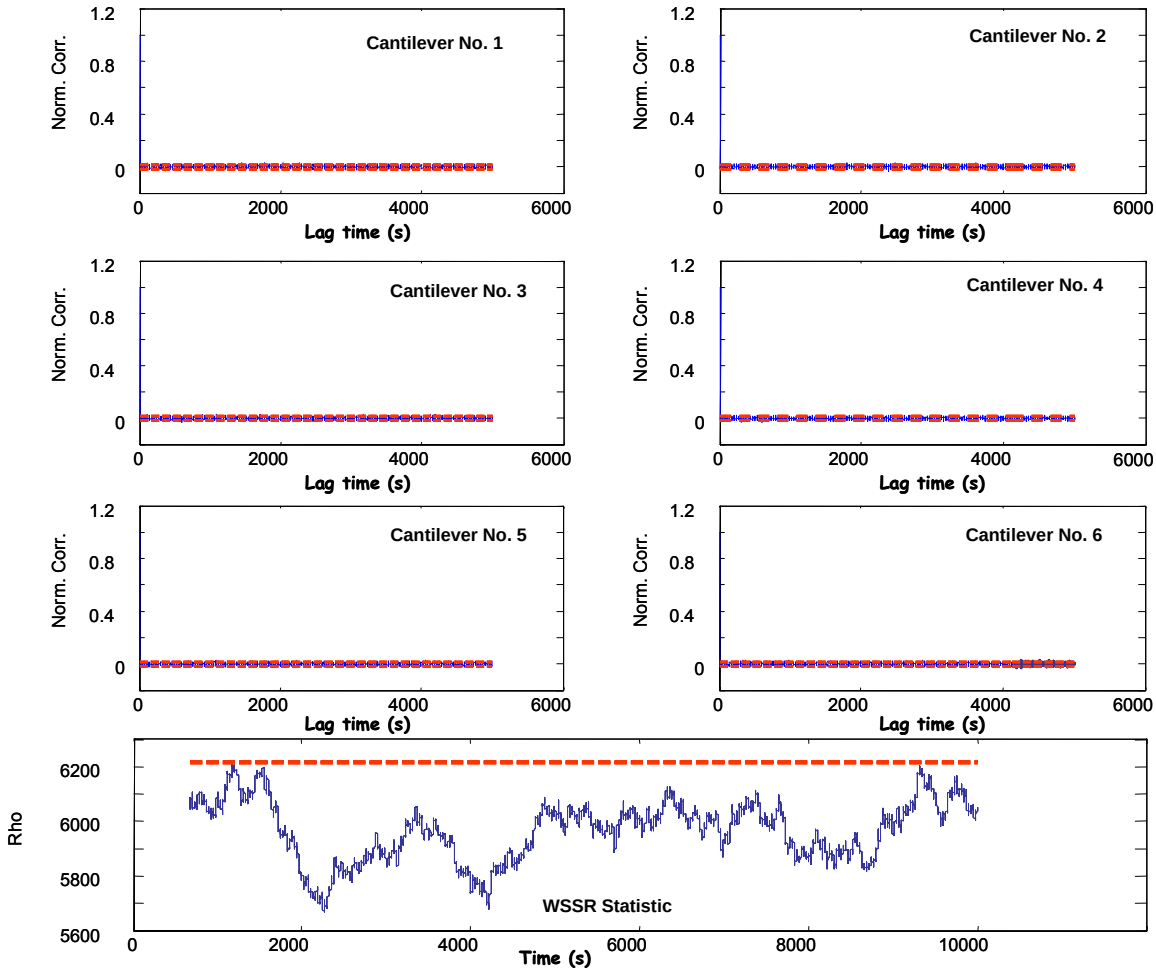

Fig. 6. Optimality Tests: Cantilever Array Zero-Mean/Whiteness and Weighted-Sum Squared Residual (WSSR) Statistic.

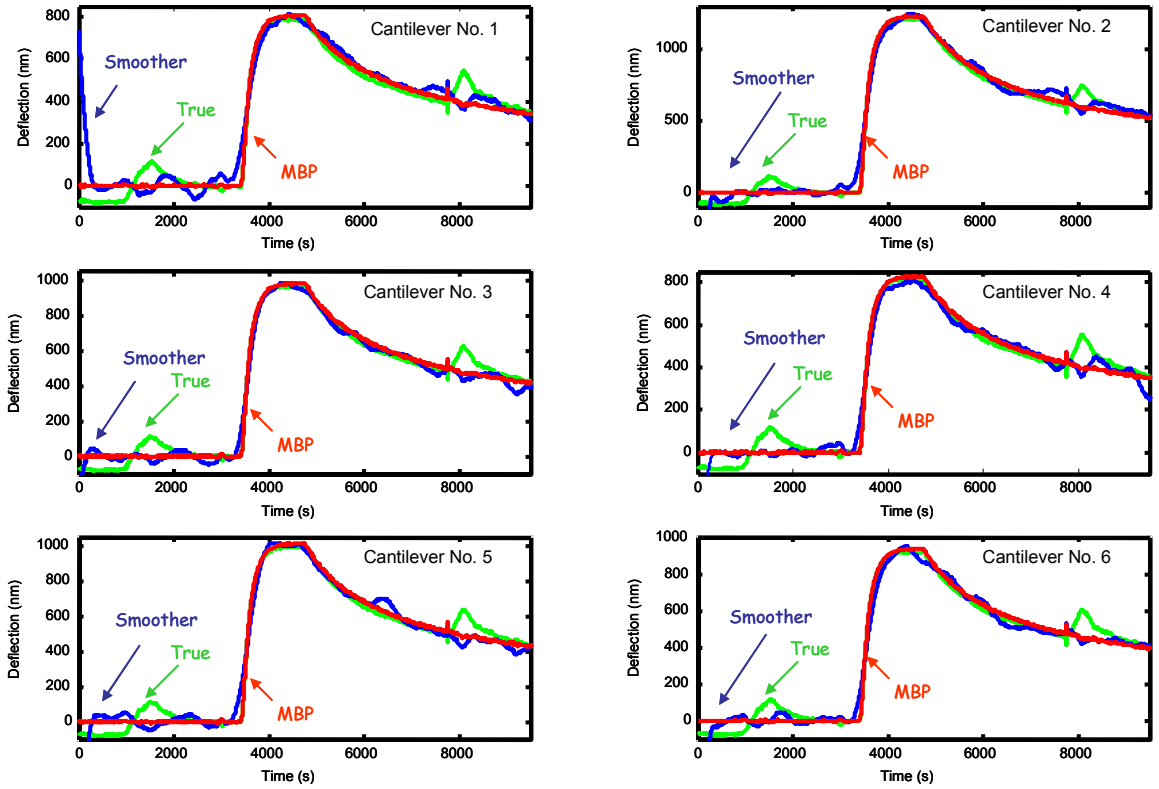

Fig. 7. MBP and Smoother Enhancement of the Noisy (*-20 dB* SNR) Synthesized Deflection Measurements: True Deflection (with temperature data), Smoothed and MBP Estimates.

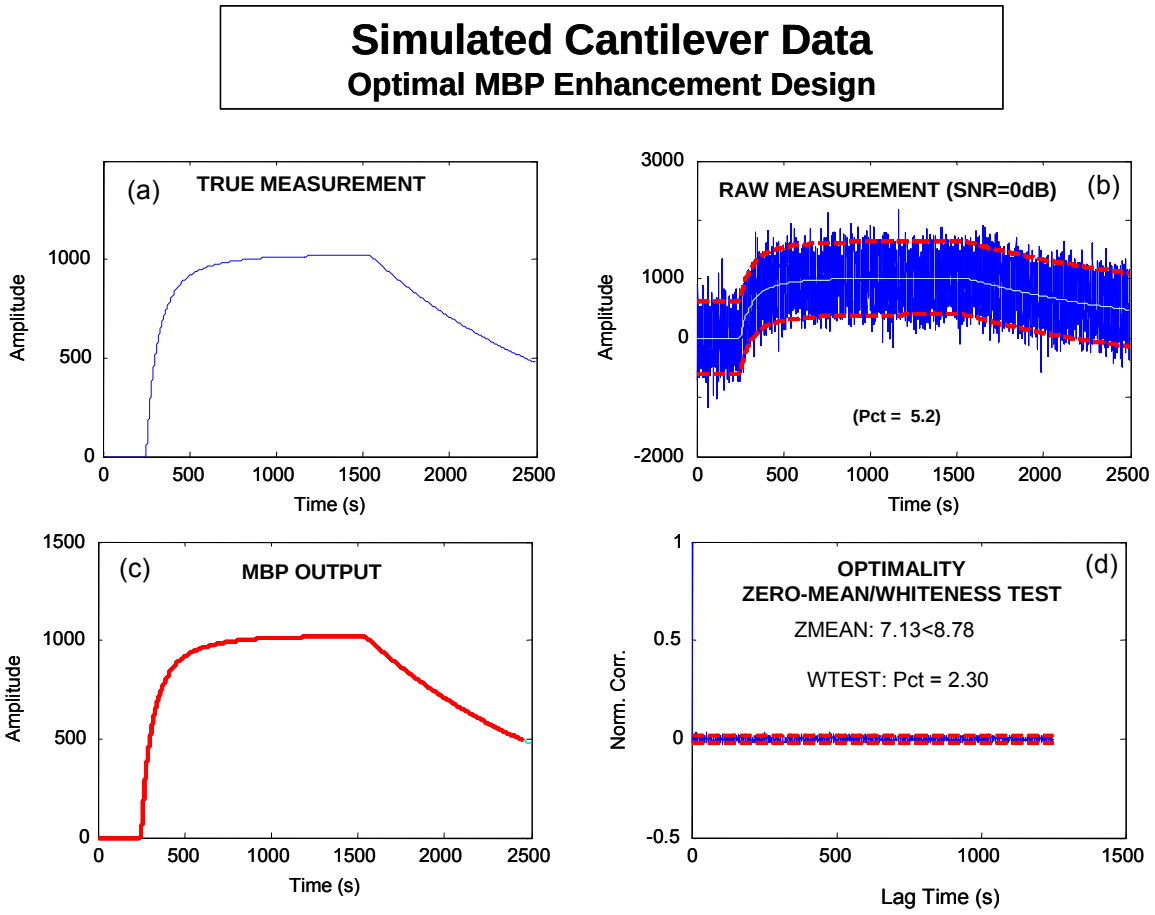

Fig. 8. MBP Design for Simulated Average Cantilever Data (*0 dB SNR*): (a) True measurement. (b) Simulated Gauss-Markov deflection measurement with bounds. (c) Enhanced deflection (MBP output). (d) Optimality tests (zero-mean/whiteness) results.

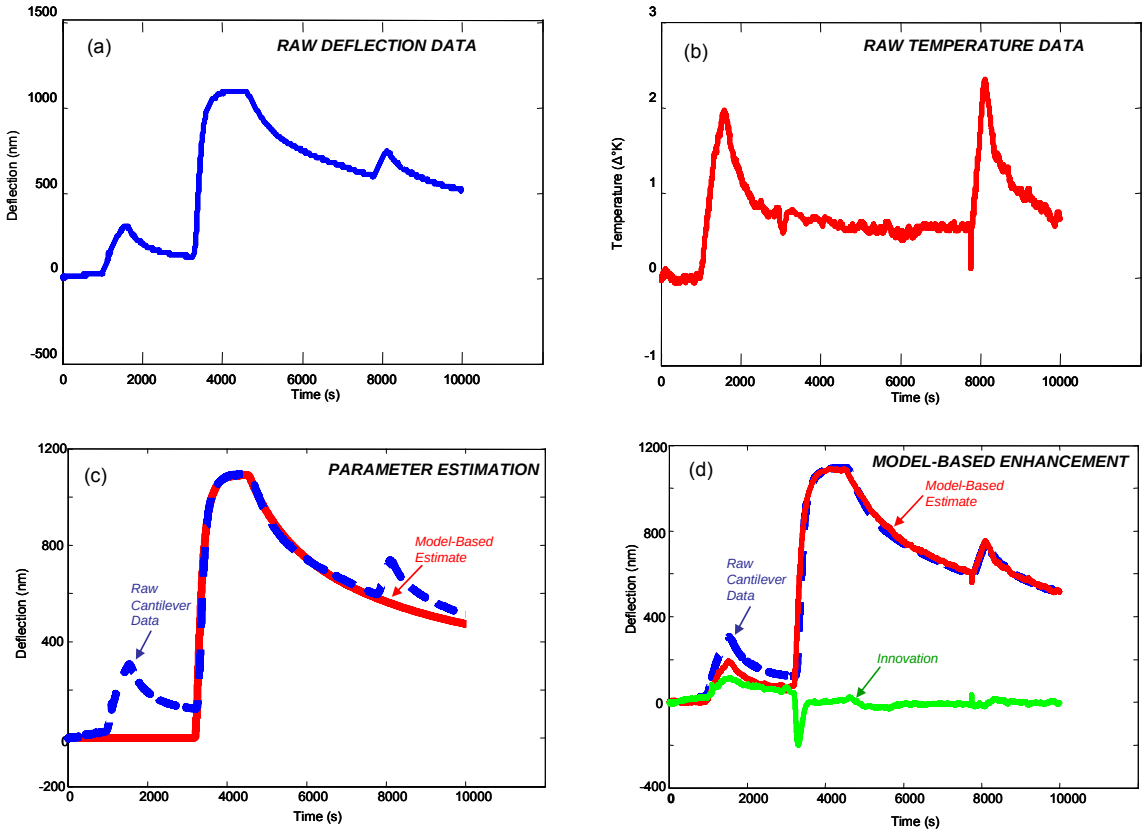

Fig. 9. Average Cantilever MBP Application to Measured Deflection Data. (a) Raw deflection data. (b) Raw temperature profile data. (c) Model-based parameter estimation fit and parameters. (d) Model-based enhancement including temperature.

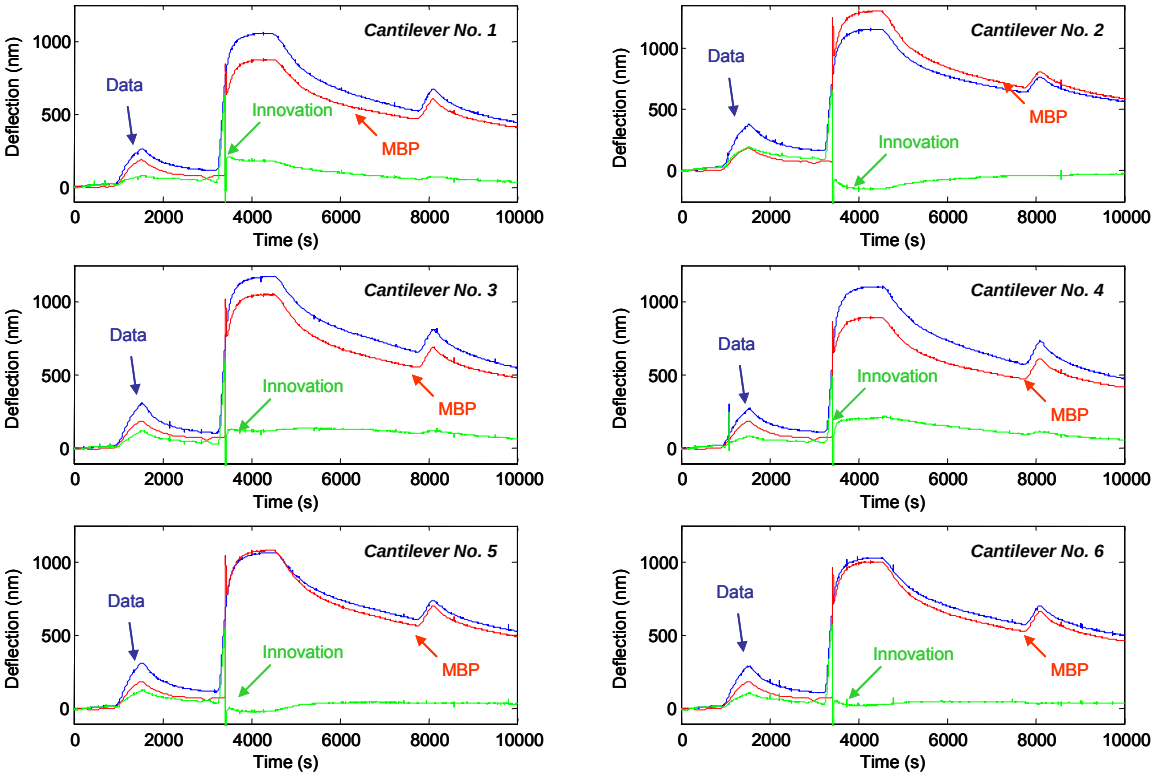

Fig. 10. MBP of Experimental Cantilever Array Data: Raw, Enhanced (MBP) and Residual (Innovation) results for each lever.

Table I: Parameters Used in Model-based Processor

Parameter	Value
E, Young's modulus for Si cantilever, Pa	1.5×10^{11}
ν, Poisson's ratio for Si cantilever, unitless	0.23
l, cantilever length, μm	500
W, cantilever width, μm	100
δ, cantilever thickness, μm	1

Table II: Cantilever Parameter Estimation for 2-Mercaptotethanol C_2H_6OS (1.4×10^{-2} M) in Water

CANTILEVER	$k_a(10^{-3})(s^{-1})$	$k_d(10^{-4})(s^{-1})$	$\Gamma_{max}(10^{15}$ molecules $cm^{-2})$
1	4.66	5.14	1.27
2	4.61	5.58	1.32
3	4.47	4.36	1.35
4	4.61	4.75	1.26
5	4.34	4.41	1.21
6	4.79	4.76	1.16
AVERAGE	4.6	4.8	1.3

Table III. MBP Optimality Zero-Mean/Whiteness Test Results

Cantilever	Mean	Bound	Whiteness (% out)	Pass/Fail
No. 1	7.64	16.7	4.25	P
No. 2	7.81	16.6	4.48	P
No. 3	11.6	16.9	4.39	P
No. 4	8.98	16.5	3.59	P
No. 5	1.93	16.8	4.51	P
No. 6	4.16	16.6	4.34	P

Table IV: MBP/Smoother Performance Analysis

SNR_{in} (dB)	0	0	-20	-20	-40	-40
Lever	SNR_o (Smt)	SNR_o (MBP)	SNR_o (Smt)	SNR_o (MBP)	SNR_o (Smt)	SNR_o (MBP)
No. 1	44.0	79.9	36.5	79.9	17.6	79.9
No. 2	46.0	87.2	40.2	87.2	26.3	87.2
No. 3	44.9	83.3	44.5	83.3	23.5	83.3
No. 4	45.2	80.3	37.9	80.3	17.3	80.3
No. 5	44.8	83.8	39.8	83.8	22.9	83.8
No. 6	45.9	82.4	40.0	82.4	24.0	82.4
AVG	45.1	82.8	39.8	82.8	21.9	82.8
Avg Gain		+37.7		+ 43.0		+60.9